

## Learning-Based Robust Observer Design for Coupled Thermal and Fluid Systems

Koga, S.; Benosman, M.; Borggaard, J.

TR2019-067 July 11, 2019

### Abstract

We present a learning-based robust observer design for thermal-fluid systems, pursuing an application to efficient energy management in buildings. The model is originally described by Boussinesq equations which is given by a system of two coupled partial differential equations (PDEs) for the velocity field and temperature profile constrained to incompressible flow. Using proper orthogonal decomposition (POD), the PDEs are reduced to a set of nonlinear ordinary differential equations (ODEs). Given a set of temperature and velocity point measurements, a nonlinear state observer is designed to reconstruct the entire state under the error of initial states, and model parametric uncertainties. We prove that the closed loop system for the observer error state satisfies an estimate of L2 norm in a sense of locally input-to-state stability (LISS) with respect to parameter uncertainties. Moreover, the uncertain parameters estimate used in the designed observer are optimized through iterations of a data-driven extremum seeking (ES) algorithm. Numerical simulation of a 2D Boussinesq PDE illustrates the performance of the proposed adaptive estimation method.

*American Control Conference (ACC)*

This work may not be copied or reproduced in whole or in part for any commercial purpose. Permission to copy in whole or in part without payment of fee is granted for nonprofit educational and research purposes provided that all such whole or partial copies include the following: a notice that such copying is by permission of Mitsubishi Electric Research Laboratories, Inc.; an acknowledgment of the authors and individual contributions to the work; and all applicable portions of the copyright notice. Copying, reproduction, or republishing for any other purpose shall require a license with payment of fee to Mitsubishi Electric Research Laboratories, Inc. All rights reserved.



# Learning-Based Robust Observer Design for Coupled Thermal and Fluid Systems

Shumon Koga, Mouhacine Benosman, Jeff Borggaard

**Abstract**—We present a learning-based robust observer design for thermal-fluid systems, pursuing an application to efficient energy management in buildings. The model is originally described by Boussinesq equations which is given by a system of two coupled partial differential equations (PDEs) for the velocity field and temperature profile constrained to incompressible flow. Using proper orthogonal decomposition (POD), the PDEs are reduced to a set of nonlinear ordinary differential equations (ODEs). Given a set of temperature and velocity point measurements, a nonlinear state observer is designed to reconstruct the entire state under the error of initial states, and model parametric uncertainties. We prove that the closed loop system for the observer error state satisfies an estimate of  $L_2$  norm in a sense of locally input-to-state stability (LISS) with respect to parameter uncertainties. Moreover, the uncertain parameters estimate used in the designed observer are optimized through iterations of a data-driven extremum seeking (ES) algorithm. Numerical simulation of a 2D Boussinesq PDE illustrates the performance of the proposed adaptive estimation method.

## I. INTRODUCTION

Thermal and fluid systems have been intensively studied for numerous applications in science and engineering processes. For instance, an efficient energy management for heating, ventilation, and air conditioning (HVAC) systems has been a priority research topic for many countries due to its huge energy consumption impact [4].

One of the important problems in HVAC management is to estimate the entire spatial profile of the airflow and temperature under a limited number of sensors placed at some locations in buildings. Such a state estimation for Navier Stokes (NS) equations has been investigated in a number of literatures in the recent decade. In [6], an infinite dimensional Kalman filter is designed for a linearized NS equation around the velocity field of interest. Their approach showed good performance as a first contribution to fluid estimation, however, there are two issues from the perspective of real implementation. One is the linearization assumption of NS equations, can produce a low fidelity fluid model. A second drawback is the high computational cost for the discretization of the infinite dimensional filter. To improve these issues, in [8], the authors developed a POD-based model reduction for NS equations, and designed extended

Kalman filter for the state estimation, which illustrated the effective results on estimated velocity profile. The later work on state estimation for POD-ROM of NS equations can be found in [9], [12].

For higher fidelity models of the NS equation which include the effect of buoyancy forces driven by the density change via temperature dependence. The dynamics of the temperature profile is also described from the conservation of energy, which formulates the Boussinesq equations as a coupled thermal and fluid systems. Due to the coupled non-linearity of two PDEs, the design and analysis of Boussinesq equations is highly challenging problem especially for 2D and 3D domains. Moreover, as presented in [10], POD-based model reduction might lose the stability property of the state variables, which is caused by the truncation of higher order modes serving as a stabilizing factor.

The stable model reduction for Boussinesq equations is developed in [2] by introducing a new closure model, which robustly stabilizes the reduced order model. The authors prove the robust stability of the closure model with respect to the parameters uncertainty using Lyapunov analysis. Furthermore, the gains in the closure terms are auto-tuned by learning-based extremum seeking (ES) algorithm to minimize the errors between the true model solution and the ROM solution. The convergence analysis of ES is established in [11] by means of singular perturbation and averaging theorem, and an approach to apply ES for parameter auto-tuning in POD-ROM is originated in [3]. The results in [2] illustrate a good performance in improving solution prediction for laminar flows, however, the method relies on the accurate knowledge of the initial velocity and temperature profiles, which can be relaxed by state estimation technique utilizing sparse measurements obtained through a few sensors.

There are two contributions in this paper. First, we have investigated the robustness of the designed observer for POD-ROM of Boussinesq equation with respect to the uncertainty of viscosity by proving input-to-state stability (ISS) in a local sense using Lyapunov method. The observer gain is designed via LMI approach to satisfy a condition for ISS proof. Second, as in [2], the online estimation of the uncertain viscosity parameter is implemented using a data-driven extremum seeking.

This paper is structured as follows. In Section II, the physical model of thermal and fluid systems is introduced by means of Boussinesq equations, and its POD-ROM is derived. Section III is devoted to the observer design for POD-ROM, where we provide the robustness analysis with

S. Koga, intern at MERL, is with the Department of Mechanical and Aerospace Engineering, U.C. San Diego, 9500 Gilman Drive, La Jolla, CA, 92093-0411, skoga@ucsd.edu

M. Benosman is with Mitsubishi Electric Research Laboratories (MERL), Cambridge, MA, 02139 benosman@ieee.org

J. Borggaard is with the Interdisciplinary Center for Applied Mathematics, Virginia Tech, Blacksburg, VA, 24061 jborggaard@vt.edu

respect to parameter uncertainty. In Section IV, the online estimation of the uncertain parameter in the designed observer is performed by ES as an iterative learning estimation, and Section V presents the numerical verification of the proposed method for 2-D Boussinesq equations. The paper ends with a conclusion and future works, as stated in Section VI.

## II. MODELLING OF THERMAL AND FLUID SYSTEMS

### A. Boussinesq equations and normalization

We focus on the dynamics of the velocity field  $\mathbf{v}(x, t) : \Omega \times \mathbb{R}^+ \rightarrow \mathbb{R}^3$  and the temperature profile  $T(x, t) : \Omega \times \mathbb{R}^+ \rightarrow \mathbb{R}$ , where  $x$  denotes the spatial coordinate  $x \in \Omega$ , and  $t \geq 0$  denotes the time. The spatial domain  $\Omega$  can be two or three dimensional space. The governing equations are described by Navier-Stokes equation with the condition of incompressible flow and the conservation of the energy through the heat transfer, which leads to the following coupled system

$$\rho \left( \frac{\partial \mathbf{v}}{\partial t} + \mathbf{v} \cdot \nabla \mathbf{v} \right) = -\nabla p + \nabla \cdot \tau(\mathbf{v}) + \rho \mathbf{g}, \quad (1)$$

$$\nabla \cdot \mathbf{v} = 0, \quad (2)$$

$$\rho c_p \left( \frac{\partial T}{\partial t} + \mathbf{v} \cdot \nabla T \right) = \nabla \cdot (\kappa \nabla T) \quad (3)$$

where  $\rho$  is the density profile,  $p$  is the pressure field,  $\tau(\mathbf{v})$  is the viscous stress,  $c_p$  is the constant heat capacity,  $\kappa$  is the constant thermal conductivity, and  $\mathbf{g} = -g\mathbf{e}_3$  is the gravitational force. In Boussinesq approximation, the buoyancy force is driven by changes in density  $\rho = \rho_0 + \Delta\rho$  from the nominal density  $\rho_0$ , and the density change is modeled as perturbations from the nominal temperature  $T_0$  using the perfect gas law  $\Delta\rho\mathbf{g} = -\rho_0\beta(T-T_0)\mathbf{g}$ ,  $\beta = 1/T_0$ , and the constant term  $\rho_0\mathbf{g}$  is absorbed into the pressure. The viscous stress is governed by  $\tau(\mathbf{v}) = \rho\nu(\nabla\mathbf{v} + \nabla\mathbf{v}^T)$  with kinematic viscosity  $\nu$ . By introducing a characteristic length  $L$ , characteristic velocity  $\mathbf{v}_0$ , wall temperature  $T_w$ , we define the following normalized states

$$\tilde{x} = \frac{x}{L}, \quad \tilde{t} = \frac{t\mathbf{v}_0}{L}, \quad \tilde{v} = \frac{v}{v_0}, \quad (4)$$

$$\tilde{p} = \frac{p}{\rho v_0^2}, \quad \tilde{T} = \frac{T - T_0}{T_w - T_0} \quad (5)$$

Using these variables, PDEs (1)–(3) can be reduced to the following (we dropped the tilde notation)

$$\frac{\partial \mathbf{v}}{\partial t} + \mathbf{v} \cdot \nabla \mathbf{v} = -\nabla p + \nabla \cdot \tau(\mathbf{v}) + \frac{\text{Gr}}{\text{Re}^2} T \mathbf{e}_3, \quad (6)$$

$$\nabla \cdot \mathbf{v} = 0, \quad (7)$$

$$\frac{\partial T}{\partial t} + \mathbf{v} \cdot \nabla T = \nabla \cdot \left( \frac{1}{\text{RePr}} \nabla T \right) \quad (8)$$

where we defined Reynolds number  $\text{Re} = \frac{v_0 L}{\nu}$ , Grashof number  $\text{Gr} = \frac{g\beta(T_w - T_0)L^3}{\nu^2}$ , and Prandtl number  $\text{Pr} = \frac{\nu}{k/\rho_0 c_p}$ .

### B. POD Model Reduction

Following Galerkin projection onto the subspace spanned by the POD basis functions, we have

$$\mathbf{v}^{pod}(x, t) = \mathbf{v}_0(x) + \sum_{i=1}^{r_v} q_i(t) \phi_i^v(x), \quad (9)$$

$$T^{pod}(x, t) = T_0(x) + \sum_{i=r_v+1}^{r_v+r_T} q_i(t) \phi_i^T(x) \quad (10)$$

where  $\mathbf{v}_0(x)$  and  $T_0(x)$  are the steady-state solution to (1)–(3),  $\phi_i^v(x)$  and  $\phi_i^T(x)$  are POD basis functions given by

$$\phi_i^v(x) = \frac{1}{t_f} \int_0^{t_f} (\mathbf{v}_{sim}(x, t) - \mathbf{v}_0(x)) w_i(t) dt, \quad (11)$$

for  $i = 1, \dots, r_v$ , and

$$\phi_i^T(x) = \frac{1}{t_f} \int_0^{t_f} (T_{sim}(x, t) - T_0(x)) w_i(t) dt, \quad (12)$$

for  $i = r_v + 1, \dots, r_v + r_T$ , with the orthogonal weight functions  $w_i(t)$  satisfying  $\int_0^{t_f} w_i(t) w_j(t) dt = 0$  if  $i \neq j$ . The coefficients  $q_i(t)$  in (9) and (10) are the dynamical states representing the POD-ROM of the Boussinesq equations. By defining the state vector  $q(t) = [q_1(t), q_2(t), \dots, q_{r_v+r_T}(t)]^T$ , we obtain the following ODE (see [2] for the detailed derivation)

$$\dot{q}(t) = \mu D q(t) + [C q(t)] q(t) + b \quad (13)$$

where  $\mu > 0$  is the viscosity  $\mu = \frac{1}{\text{Re}}$ ,  $D$  is a negative definite diffusion matrix with diagonal blocks corresponding to the viscous stress and thermal diffusion, and  $C$  is a three-dimensional tensor corresponding the convection terms in (6) and (8).

*Remark 1:* While the original PDEs (1)–(3) is a stable system (in the sense of boundedness) from our knowledge on thermal and fluid dynamics, the obtained POD-ROM (13) might become unstable depending on the strength of the quadratic nonlinearity  $[C q(t)] q(t)$  and the constant term  $b$  relative to the damping effect  $\mu D q(t)$ . We study the effect of  $\mu$  on the boundedness of the solution to (13) in the next lemma.

*Lemma 1:* For a viscosity coefficient satisfying

$$\mu \geq \frac{2}{\underline{d}} \max \left\{ \sqrt{c_{max} b_{max}}, c_{max} \|q_0\| \right\} \quad (14)$$

where  $\underline{d} := \lambda_{min}(-D) > 0$ ,  $c_{max} = \|C\|_F$ ,  $b_{max} = \|b\|$ , the following explicit bound holds

$$\|q\| \leq Y^* + \frac{\bar{b}}{c_{max} + \left( \frac{\bar{b}}{\|q_0\| - Y^*} - c_{max} \right) e^{\bar{b}t}} \quad (15)$$

where  $\bar{b} = \sqrt{\mu^2 \underline{d}^2 - 4b_{max} c_{max}}$ , and  $Y^* = \frac{\mu \underline{d} - \bar{b}}{2c_{max}}$ . Moreover, the solution is uniformly bounded by a positive constant  $M = \frac{\mu \underline{d}}{2c_{max}}$ , i.e.,  $\|q\| \leq M$ .

*Proof:* The proof has been omitted due to space constraints, however, it will be included in a longer journal version of this work. ■

### III. ROBUSTNESS OF NONLINEAR OBSERVER IN LOCAL ISS SENSE

To solve for the POD-ROM in (13), the values of the viscosity parameter  $\mu$  and the initial conditions  $q(0)$  are needed, however, in most applications they are uncertain. Instead, we can allocate thermal and velocity sensors to measure some partial states of the system, which can be formulated as a linear map from the POD states

$$y(t) = Hq(t), \quad (16)$$

where  $H \in \mathbb{R}^{m \times n}$  is a measurement matrix given by the sensor placement. Then, to assimilate the model (13) with the acquired sensor data, the state estimator is designed to reconstruct the entire state  $q(t)$  from the measured data, which enables to estimate the velocity field  $v^{pod}(x, t)$  and the temperature profile  $T^{pod}(x, t)$  for all  $x$ . A well-known design is Luenberger-like observer which is constructed as a copy of the plant plus the injection of the measurement error states, written by

$$\dot{\hat{q}}(t) = \hat{\mu}D\hat{q}(t) + [C\hat{q}(t)]\hat{q}(t) + b + L(y(t) - H\hat{q}(t)), \quad (17)$$

where  $\hat{q}(t)$  is the estimation of states  $q(t)$ ,  $\hat{\mu}$  is the estimated values of  $\mu$ , and  $L \in \mathbb{R}^{n \times m}$  is the observer gain to be determined. For analysis purposes, we impose the following assumption.

*Assumption 1:* The lower bound of the viscosity  $\mu$  is known, i.e.,  $\underline{\mu} \leq \mu$ . Furthermore, our estimated value of the viscosity also satisfies  $\underline{\mu} \leq \hat{\mu}$ .

Let  $\tilde{q}(t)$  be the estimation error state defined by

$$\tilde{q}(t) := q(t) - \hat{q}(t). \quad (18)$$

The ideal performance of the observer is characterized by some sort of the stability property of the estimation error  $\tilde{q}(t)$ . Subtraction of the estimator (17) from the system (13) yields the following estimation error dynamics

$$\begin{aligned} \dot{\tilde{q}}(t) = & (\underline{\mu}D - LH)\tilde{q}(t) + \mu_+D\tilde{q}(t) + \tilde{\mu}Dq(t) \\ & + [C\tilde{q}(t)]q(t) + [Cq(t)]\tilde{q}(t) - [C\tilde{q}(t)]\tilde{q}(t). \end{aligned} \quad (19)$$

where  $\mu_+ := \mu - \underline{\mu} > 0$ , and  $\tilde{\mu} = \mu - \hat{\mu}$ . Our main result is presented in the following theorem.

*Theorem 1:* Consider the estimation error system (19). Let the observer gain  $L$  be designed so that the matrix  $\underline{\mu}D - LH$  is Hurwitz and satisfies the following property

$$\lambda_{min}(Q) \geq 16c_{max}M\lambda_{max}(P), \quad (20)$$

where  $P = P^T > 0$  and  $Q = Q^T > 0$  are the solutions of Lyapunov equation  $P(\underline{\mu}D - LH) + (\underline{\mu}D - LH)^T P^T = -Q$ . Then, there exist positive constants  $\rho_0 > 0$ ,  $\rho_u > 0$ , and a class  $\mathcal{KL}$  function  $\beta$  and a class  $\mathcal{K}$  function  $\gamma$  such that if  $|\tilde{q}(0)| < \rho_0$  and  $|\tilde{\mu}| < \rho_u$  then the following estimate of the norm holds :

$$\|\tilde{q}(t)\| \leq \beta(\|\tilde{q}(0)\|, t) + \gamma(|\tilde{\mu}|), \quad (21)$$

which guarantees the local input-to-state stability (LISS) of the estimation error system with respect to the parameter uncertainty. Moreover, by defining  $\bar{\sigma} = \frac{\lambda_{min}(Q)}{4\sqrt{\lambda_{min}(P)}\sqrt{\lambda_{max}(P)}}$ ,

$\bar{\delta} = c_{max} \frac{\lambda_{max}(P)}{\lambda_{min}(P)^{3/2}}$ , and  $\bar{\alpha} = \frac{M\lambda_{max}(P)}{\sqrt{\lambda_{min}(P)}}\lambda_{max}(-D)$ , the explicit formulation for the constant bound and functions are obtained by  $\rho_u = \frac{\lambda_{min}(Q)}{4\sqrt{\lambda_{min}(P)}\sqrt{\lambda_{max}(P)}}$ ,  $\rho_0 = \frac{\bar{\sigma}}{4\bar{\delta}}$ , and

$$\beta(\|q_0\|, t) = 4\|q_0\|e^{-\frac{\bar{\sigma}}{2}t}, \quad (22)$$

$$\gamma(u) = 5 \frac{\bar{\sigma} - \sqrt{\bar{\sigma}^2 - 4\sqrt{2}\bar{\delta}\bar{\alpha}u}}{2\bar{\delta}}, \quad (23)$$

which ensures the exponentially LISS.

*Proof:* We consider the candidate of LISS Lyapunov function  $V$  defined by

$$\tilde{V} = \tilde{q}^T P \tilde{q} \quad (24)$$

Note  $\lambda_{min}(P)\tilde{q}^T \tilde{q} \leq \tilde{V} \leq \lambda_{max}(P)\tilde{q}^T \tilde{q}$ . Taking the time derivative of (24) along the solution of (19), we obtain

$$\begin{aligned} \dot{\tilde{V}} = & -\tilde{q}^T Q \tilde{q} + 2\tilde{\mu}q^T D^T P \tilde{q} - \tilde{\mu}\tilde{q}^T (DP + PD)\tilde{q} \\ & + 2\mu_+\tilde{q}^T D \tilde{q} + 2([C\tilde{q}]q)^T P \tilde{q} + 2([Cq]\tilde{q})^T P \tilde{q} \\ & - 2([C\tilde{q}]\tilde{q})^T P \tilde{q} \end{aligned} \quad (25)$$

Owing to the negative definiteness of  $D < 0$  and positivity of  $\mu_+ > 0$ , it holds  $\mu_+\tilde{q}^T D \tilde{q} < 0$ . Furthermore, by Cauchy-Schwarz inequality,

$$\begin{aligned} ([C\tilde{q}]q)^T P \tilde{q} & \leq \| [C\tilde{q}]q \| \cdot \| P \tilde{q} \| \\ & \leq c_{max}\lambda_{max}(P)M\|\tilde{q}\|^2 \end{aligned} \quad (26)$$

where we used  $\|q\| \leq M$  given in Lemma 1. Using the same technique to all terms in the last line in (25), and defining  $\bar{d} := \lambda_{max}(-D) > 0$ , the inequality (25) leads to

$$\begin{aligned} \dot{\tilde{V}} & \leq -\lambda_{min}(Q)\|\tilde{q}\|^2 + 2M\bar{d}\lambda_{max}(P)\|\tilde{q}\|\|\tilde{\mu}\| \\ & + 4c_{max}\lambda_{max}(P)M\|\tilde{q}\|^2 + 2c_{max}\lambda_{max}(P)\|\tilde{q}\|^3 \\ & + 2\lambda_{min}(P)\bar{d}\|\tilde{\mu}\|\|\tilde{q}\|^2 \\ & \leq -\frac{\lambda_{min}(Q)}{2}\|\tilde{q}\|^2 + 2c_{max}\lambda_{max}(P)\|\tilde{q}\|^3 \\ & + \left( 2M\bar{d}\lambda_{max}(P)\|\tilde{\mu}\| - \frac{\lambda_{min}(Q)}{4}\|\tilde{q}\| \right) \|\tilde{q}\| \\ & + \left( 4c_{max}\lambda_{max}(P)M - \frac{\lambda_{min}(Q)}{4} \right) \|\tilde{q}\|^2 \\ & + 2\lambda_{min}(P)\bar{d}\|\tilde{\mu}\|\|\tilde{q}\|^2. \end{aligned} \quad (27)$$

Therefore, by designing the observer gain  $L$  such that the condition (20) holds, we can state that if

$$|\tilde{\mu}| \leq p\|\tilde{q}\| \quad (28)$$

where  $p := \frac{\lambda_{min}(Q)}{16M\bar{d}\lambda_{max}(P)}$ , then (27) leads to

$$\dot{\tilde{V}} \leq -\sigma\|\tilde{q}\|^2 + \delta\|\tilde{q}\|^3, \quad (29)$$

where  $\sigma = \frac{\lambda_{min}(Q)}{2}$ ,  $\delta = 2\lambda_{max}(P)(c_{max} + \bar{d}p)$ . Applying Theorem 1 in [7], we can conclude the local ISS w.r.t. the parameter uncertainty  $\mu$ . Applying the similar technique in proof of Lemma 1 to (27), we can further obtain the explicit bound by the solution of Riccati differential equation, which derive the explicit formulation of the functions  $\beta$  and  $\gamma$  in LISS. ■

#### IV. PARAMETRIC UNCERTAINTY ESTIMATION BY AN EXTREMUM SEEKING ALGORITHM

To enhance the performance of the state observer based on the measured value, the uncertain viscosity parameter estimate used in the observer should be corrected through learning iterations. The learning cost function to minimize at every iteration is an error between the measured value and its estimate, which is formulated as

$$Q(\hat{\mu}) = \int_0^{t_f} (y(t) - H\hat{q}(t))^T R (y(t) - H\hat{q}(t)) dt, \quad R > 0. \quad (30)$$

Since the estimate of the parameter  $\hat{\mu}$  affects the observer state  $\hat{q}$ , the cost function  $Q$  is an implicit function of  $\hat{\mu}$ . Following [3], we impose the following assumptions on the cost function.

*Assumption 2:* The cost function  $Q(\cdot)$  in (30) has a local minimum at  $\hat{\mu} = \mu$ .

*Assumption 3:* The cost function in (30) is analytic and its variation with respect to  $\hat{\mu}$  is bounded in the neighborhood of  $\mu$ , i.e.,  $\|\nabla_{\hat{\mu}} Q(\delta\mu)\| \leq \xi_2$ ,  $\xi_2 > 0$ , for all  $\delta\mu \in \mathcal{N}(\mu)$ , where  $\mathcal{N}(\mu)$  denotes a compact neighborhood of  $\mu$ .

We apply an extremum seeking algorithm as a learning method for parameter identification. Let  $\hat{\mu}^{(i)}$  be the estimate of the parameter  $\mu$  at  $i$ -th iteration, and we introduce an internal variable  $z^{(i)}$  with initial value  $z^{(1)} = \hat{\mu}^{(1)}$ . The parameters update through ES algorithm is given by

$$z^{(i+1)} = z^{(i)} + a\delta \sin\left(\omega i\delta + \frac{\pi}{2}\right) Q(\hat{\mu}^{(i)}) \quad (31)$$

$$\hat{\mu}^{(i+1)} = z^{(i+1)} + a \sin\left(\omega i\delta - \frac{\pi}{2}\right), \quad (32)$$

where the tuning parameters are  $(a, \omega, \delta)$  which are the amplitude, the frequency, and the iteration increment  $\delta > 0$ , respectively. Owing to the convergence analysis of the extremum seeking algorithm as presented for example in [11], [3], the performance of the learning-based observer is addressed in the following lemma.

*Lemma 2:* Let Assumptions 1–3 hold. Consider the POD-ROM (13) and the designed observer (17) satisfying (20). Furthermore, where the viscosity estimate  $\hat{\mu}$  is tuned by the ES algorithm (31) and (32) associated with the cost function (30) at the iteration step  $i \in \mathbb{N}$ . Then, there exists  $\xi_1 > 0$  such that the norm of the parameter estimation error and the learning cost function admit the following bounds

$$\limsup_{i \rightarrow \infty} |\hat{\mu}^{(i)} - \mu| \leq \frac{\xi_1}{\omega} + |a|, \quad (33)$$

$$\limsup_{i \rightarrow \infty} |Q(\hat{\mu}^{(i)}) - Q(\mu)| \leq \xi_2 \left( \frac{\xi_1}{\omega} + |a| \right) \quad (34)$$

Moreover, if  $\|\tilde{q}(0)\| < \rho_0$  and  $|\hat{\mu}| < \rho_u$  then the norm of the state estimation error admits the following bound

$$\limsup_{i \rightarrow \infty} \|\tilde{q}^{(i)}(t)\| \leq \beta(\|\tilde{q}_0\|, t) + \gamma \left( \frac{\xi_1}{\omega} + |a| \right) \quad (35)$$

where  $\tilde{q}^{(i)}(t) = q(t) - \hat{q}^{(i)}(t)$  with the observer state  $\hat{q}^{(i)}(t)$  in  $i$ -th iteration,  $\rho_0$ ,  $\rho_u$ ,  $\beta$ , and  $\gamma$  are defined in Theorem 1.

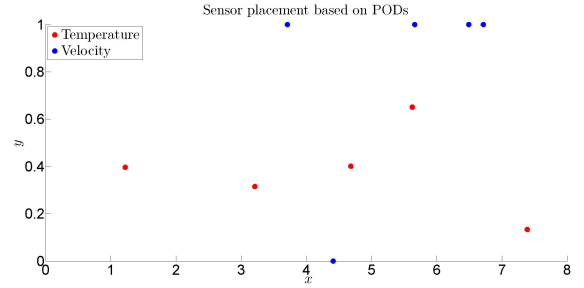


Fig. 1. Sensor placement for both temperature (red) and velocity (blue).

*Proof:* The proof of (33) and (34) is the same derivation as in [2], and hence is omitted here. Finally, taking the supremum limit in the norm bound (21) in Theorem 1, we obtain

$$\limsup_{i \rightarrow \infty} \|\tilde{q}^{(i)}(t)\| \leq \beta(\|\tilde{q}_0\|, t) + \limsup_{i \rightarrow \infty} \gamma \left( |\mu - \hat{\mu}^{(i)}| \right) \quad (36)$$

from which the norm estimate (35) is derived with the help of (33). ■

#### V. NUMERICAL SIMULATION

##### A. Input parameters

We implement the numerical simulation by setting the spatial domain as a 2-D rectangular shape, namely,  $\Omega = (0, 8) \times (0, 1)$ . The non-dimensional parameters are chosen as  $Re = 10^4$ ,  $Pr = 1$ , and  $Gr = 4 \times 10^8$ . The setup of this experiment, e.g., [2], is as follows: Two fluids of different temperatures are separated by a vertical barrier at  $x = 4$ . On the right side of the barrier we have low temperature set to 1, whereas, on the left side of the barrier we have high temperature, set to 1.5. When we remove the barrier between the two fluids, we expect the low density, warmer fluid to rise, while the high density, cooler fluid sinks. The flow is at rest initially (i.e., the vorticity and stream functions are set to zero at  $t = 0$ ) with constant temperature values for the left and right fluids. The 2-D equations were simulated using a vorticity-streamfunction formulation with no-slip boundary conditions for vorticity and adiabatic boundary conditions for temperature. We use 10 POD basis functions for the vorticity and 10 POD basis functions for the temperature variables computed from snapshots taken every  $2 \times 10^{-2}$  [s]. The simulation time is set as  $t_f = 10$  [s]. The observer gain is obtained using an LMI solver in MATLAB to ensure the existence of a positive solution to the Lyapunov equation stated in Theorem 1. The initial observer state is set as  $\hat{q}(0) = (1 + \varepsilon)q(0)$ , with setting  $\varepsilon = 0.1$ , which implies that the observer state has 10 % error on initial condition. The true viscosity is normalized as  $\mu = 1.05$ , while the initial guess of the estimated viscosity is set as  $\hat{\mu}^{(1)} = 1.00$ , which has 5% error. The learned parameter is updated through 1000 iterations. For measurements, we consider 5 sensors for temperature and 5 sensors for velocity, and they are placed, using Q-DEIM method, e.g., [5], at the locations which are

**Algorithm 1:** Iterative learning for online parameter estimation in state observer

**Input :**  $\{y_t\}_{t=0}^{t_f}$ ,  $\hat{\mu}^{(1)}$ ,  $\hat{q}_0$ ;  
 $z \leftarrow \hat{\mu}^{(1)}$ ;  
**for**  $i = 1, 2, \dots, I$ , **do**  
    **for**  $t = 0, \dots, t_f - 1$ , **do**  
         $\hat{q}_{t+1} \leftarrow f(\hat{q}_t, y_t, \hat{\mu}^{(i)})$ ;  
         $\tilde{y}_t \leftarrow y_t - H\hat{q}_t$ ;  
    **end for**  
     $Q \leftarrow \text{Trapz}(\tilde{y}_t^T \tilde{y}_t)$ ;  
     $z \leftarrow z + a\delta \sin(\omega i\delta + \frac{\pi}{2}) Q$ ;  
     $\hat{\mu}^{(i+1)} \leftarrow z + a \sin(\omega i\delta - \frac{\pi}{2})$ ;  
**end for**  
 $\hat{\mu}^{\text{ave}} \leftarrow \text{Mean}(\{\hat{\mu}^{(i)}\}_{i=0.9..I})$ ;  
**for**  $t = 0, \dots, t_f - 1$ , **do**  
     $\hat{q}_{t+1} \leftarrow f(\hat{q}_t, y_t, \hat{\mu}^{\text{ave}})$ ;  
**end for**  
**Output :**  $\hat{\mu}^{\text{ave}}$ ,  $\{\hat{q}_t\}_{t=0}^{t_f}$

depicted in Fig. 1. Then, the measurement matrix  $H$  in (16) is obtained through the POD basis functions.

*B. Algorithm for ES-based observer*

After time discretization, the dynamics of the POD ROM (13) and the designed observer (17) are described by the difference equation in the form of  $\hat{q}_{t+1} = f(\hat{q}_t, y_t, \hat{\mu})$ , for  $t = 0, 1, \dots, T_f$ , with  $\hat{q}_t = \hat{q}(t\Delta t)$ . In numerical experiment, the measured values  $\{y_t\}_{t=0}^{T_f}$  are obtained through forward simulation of the model. Using the collected measured data as inputs, we calculate the observer state  $\{\hat{q}_t\}_{t=0}^{T_f}$  with an initial guess of  $\hat{\mu}$ . Once  $\{\hat{q}_t\}_{t=0}^{T_f}$  has been obtained, the ES algorithm is implemented to update the learned parameter. We repeat this process (“run observer”  $\leftrightarrow$  “parameter update”) up to  $I$ -th iterations, where  $I$  is a chosen iteration number. After that, the averaged value of the learned parameter over the last 10 % steps is calculated, which serves as the value for the uncertain parameter estimate. Finally, we run the observer dynamics again, using the learned parameter. This procedure is stated in Algorithm 1.

*C. Simulation result*

The simulation of the learning-based observer is implemented. Fig. 2 depicts the time evolution of the first two modes in both velocity and temperature for the: true value (red), estimate before learning (green), and the estimate after learning (blue), respectively. For all of these four states, we can observe that the estimated value becomes much closer to the true value after ES-based learning of the uncertain parameter. As depicted in Fig. 3, the norm of the estimation error is converging to zero after learning (blue), while the estimation error norm before learning shows a diverging behavior. We underline here that, once the POD modes or time-coefficients have been estimated, one can easily reconstruct the full velocity and temperature profiles by lifting the time-coefficients to the  $x$ -domain via the parametrization

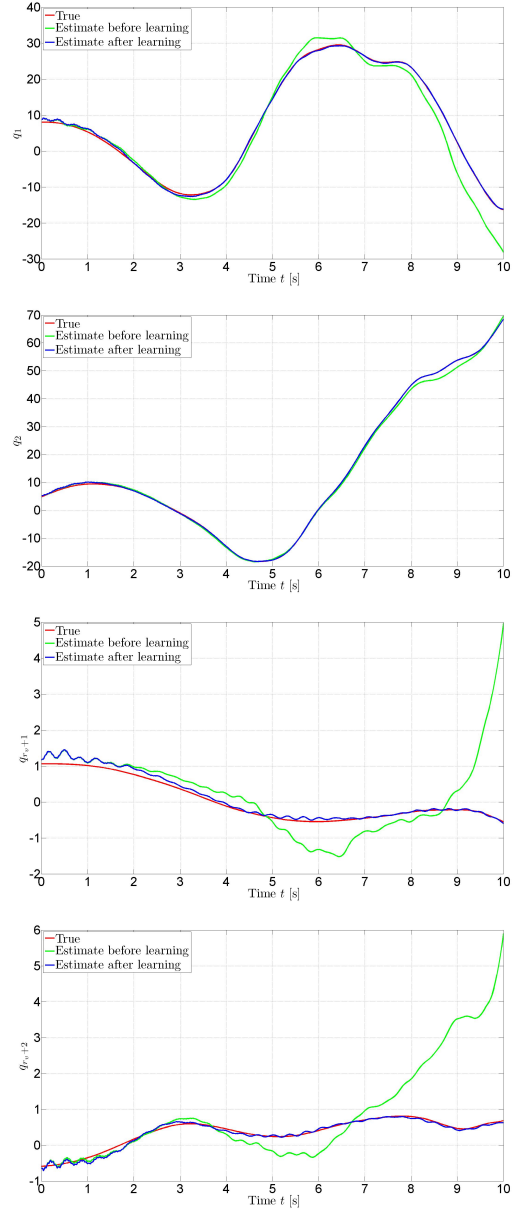


Fig. 2. Evolution of first and second modes in both velocity and temperature states of POD-ROM: True value (red), estimate before learning (green), and estimate after learning (blue). For all of the modes given here, we can observe that the estimate value is highly improved after learning the uncertain parameter.

given by (9), and (10). We have not reported here the graphs corresponding to these reconstructions, due to space limitation, however, we will report them in a longer journal version of this work.

The update of the learned parameter  $\hat{\mu}^{(i)}$  over the learning iterations is depicted in Fig. 4. While the initial guess of the parameter has 5% error, by employing ES we can observe that after 200 steps the learned parameter  $\hat{\mu}^{(i)}$  converges to the neighborhood of the true value  $\hat{\mu}$ . The amplitude of the learned parameter around the averaged value directly depends on the amplitude  $a$  of the dither signal for ES,

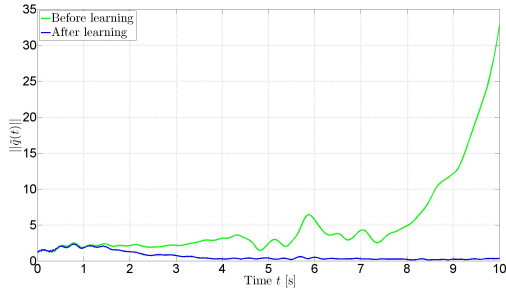


Fig. 3. Evolution of the norm of the estimation error before learning (green) and after learning (blue), which illustrates high improvement of the estimator performance through ES-based auto-tuning of parameter.

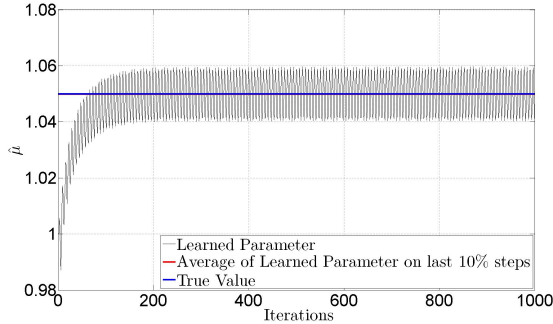


Fig. 4. Iterative learning of parameter by ES. After 200 steps, the learned parameter  $\hat{\mu}^{(i)}$  stays on neighborhood of the true value  $\mu = 1.05$ . The averaged value of the learned parameter over the last 100 steps becomes  $\hat{\mu}^{\text{ave}} = 1.05$ , same value as the true value.

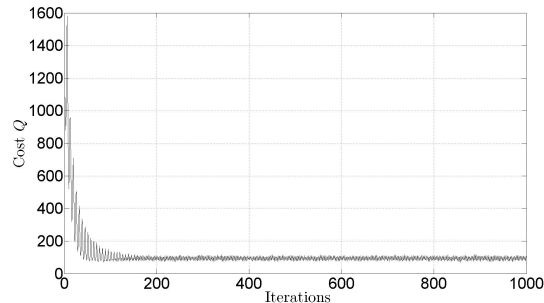


Fig. 5. Update of the cost function  $Q$  at each iteration. The value of the cost is largely decreased during the first 100 steps, and after that it almost maintains the minimum value with having a little oscillation.

which can be tuned by the user. Smaller choice of  $a$  decreases the amplitude of the learned parameter, however, the convergence speed becomes slower in general. Such a tradeoff can be dealt by performance improvement of the ES algorithm proposed in [14], which provides convergence to global optima in the presence of local extrema, this will be considered in a future work. Finally, the iterative update of the cost function is shown in Fig. 5, from which we observe the convergence to the minimum value of  $Q$  after 100 steps. Overall, the proposed method for a learning-based state estimation shows a good performance in this numerical study of the challenging 2-D Boussinesq equations.

## VI. CONCLUSIONS AND FUTURE WORK

In this paper, we develop a learning-based robust observer design for POD-ROM models of the Boussinesq equations. We prove ISS between the states estimation error and the uncertain parameters estimation error. Then, we use ES for online estimation of model parametric uncertainties. The proposed method is applied to the 2-D Boussinesq equation, which illustrates the good performance in estimating the entire POD time coefficients, i.e., the entire profile of temperature and velocity which can be obtained by lifting the POD time coefficients to the  $x$ -domain by using the POD basis functions parametrization of the temperature and velocity. In future works, we will study the case of 3-D Boussinesq equations, which correspond to a more realistic model of indoor airflows related to practical applications in HVAC systems. Another interesting, but challenging, research direction would be to bound the errors between the ROM-based estimates and the true solutions of the original PDE.

## REFERENCES

- [1] M. Arcak and P. Kokotovic, "Nonlinear observers: a circle criterion design and robustness analysis," *Automatica*, vol. 37, pp.1923-1930, 2001.
- [2] M. Benosman, J. Borggaard, O. San, and B. Kramer, "Learning-based robust stabilization for reduced-order models of 2D and 3D Boussinesq equations," *Applied Mathematical Modelling*, vol. 49, pp.162-181, 2017.
- [3] M. Benosman, *Learning-Based Adaptive Control: An Extremum Seeking Approach—Theory and Applications*. Butterworth-Heinemann, 2016.
- [4] J. Borggaard, J. A. Burns, A. Surana, and L. Zietsman, "Control, estimation and optimization of energy efficient buildings," In *2009 American Control Conference (ACC)*, pages 837-841. IEEE, 2009.
- [5] Z. Drmac and S. Gugercin, "A New Selection Operator for the Discrete Empirical Interpolation Method—Improved A Priori Error Bound and Extensions," *Methods and Algorithms for Scientific Computing*, vol. 32, num. 8, pp.631-648, 2016.
- [6] M.Chevalier, J. Hoepffner, T. R. Bewley, and D.S. Henningson, "State estimation in wall-bounded flow systems. Part 2. Turbulent flows," *Journal of Fluid Mechanics*, vol. 552, pp.167-187, 2006.
- [7] S. Dashkovskiy and A. Mironchenko, *Input-to-state stability of infinite-dimensional control systems*. Mathematics of Control, Signals, and Systems, 2013.
- [8] M. Guay and N. Harihan, "Airflow velocity estimation in building systems," In *2008 American Control Conference (ACC)*, pages 908-913. IEEE, 2009.
- [9] T. John, M. Guay, N. Harihan, and S. Narayan, "POD-based observer for estimation in Navier-Stokes flow," *Computers & chemical engineering*, vol. 34.6, pp. 965-975, 2010.
- [10] V. L. Kalb, and A. E. Deane, "An intrinsic stabilization scheme for proper orthogonal decomposition based low-dimensional models," *Physics of fluids*, vol. 19.5, 054106, 2007.
- [11] M. Krstic, and H. H. Wang, "Stability of extremum seeking feedback for general nonlinear dynamic systems," *Automatica*, vol. 36.4, pp. 595-601, 2000.
- [12] W. MacKunis, S. V. Drakunov, M. Reyhanoglu, and L. Ukeiley, "Nonlinear estimation of fluid flow velocity fields," In *50th Conference on Decision and Control (CDC)*, pages 6931-6935, 2011.
- [13] E. D. Sontag, and Y. Wang, "New characterizations of input-to-state stability," *IEEE Transactions on Automatic Control*, vol. 41, pp. 1283-1294, 1996.
- [14] Y. Tan, D.R. Nescic, I.M. Mareels, and A. Astolfi, "On global extremum seeking in the presence of local extrema," *Automatica*, vol. 45, pp. 245-251, 2009.
- [15] R. Temam, and J. Tribbia, "Open boundary conditions for the primitive and Boussinesq equations," *Journal of the Atmospheric Sciences*, vol. 60.21, pp. 2647-2660, 2003.